Cavity-enhanced second harmonic generation in a silica whispering-gallery microresonator

June 11, 2017

Centrosymmetric materials ... most significant application: surface probe... surface response is intrinsically weak, so several methods are used to enhanced surface SHG (e.g. plasmonic)... cavity boosts the intensity of light, making it a good platform for nonlinear optics...cavity enhanced SHG... Recently, SHG with bare silica cavity (Asano OL)...

Here, second harmonic, originating from symmetry breaking at the surface and bulk multipole response (fig.1 **b**), is observed under the continuous wave pump below 1 mW in a WGM microsphere made of centrosymmetric material. An unprecedented conversion efficiency of 0.049% W^{-1} benefits from doubly resonant enhancement of ultrahigh Q modes (phase-matching condition[also know as perfect phase matched]), which is achieved by thermal effect and optical Kerr effect. The work enriches the nonlinear toolbox of microcavity photonics and largely extends the emission range of silica microresonators with ultralow pump power, making it possible to push the frequency conversion process down to the quantum regime[refs in Asano OL]. More significantly, the fruitful surface SHG and SFG detection methods can be introduced into (bridged with?) the sensitive microcavity sensing, which enables surface-specific detection with low pump power and high sensitivity.

In the experiment, a silica microsphere (diameter ~ 62 μm) is pumped through a tapered optical fiber (waist diameter ~ 1 μm) at 1550 nm band [1, 2], as shown in fig.1 **a**. To collect SH signal efficiently, a second fiber taper (waist diameter ~ 0.5 μm) designed for 780 nm band is incorporated into the system. The intrinsic quality factor (Q) for the pumped cavity mode is 4.8×10^7. Figure 1**c** shows a typical SH spectrum from the electron-multiplying CCD (EMCCD) and the corresponding pump spectrum from the optical spectrum analyzer (OSA). The SH signal of 777.75 nm appears when pumped at 1555.14 nm, which deviates only 0.023% from the expected wavelength, falling into the resolution tolerance of OSA and EMCCD. Note that stimulated Raman scattering and parametric oscillation do not occur because their thresholds are far above the pump power in the experiment. Third harmonic generation is also absent due to the phase mismatch in the nonlinear optical process. Moreover, SH signals arise in the full range when cavity modes are pumped from 1545 nm to 1565 nm, as shown in Fig.1d. Among the occurrence of SH, a maximum signal power of 5 nW can be obtained via the signal fiber. To compare the collecting efficiency of the two fibers, we optimize the fiber-cavity coupling so that the SH signal from the pump fiber is also observable but the maximum power is still over one order of magnitude weaker than that from the signal fiber. From either fibers, SH signal is absent when the pump is off-resonance with cavity modes, which helps to eliminate the possibility of spurious signals such as the second order diffraction of the EMCCD grating.

The doubly resonant enhancement plays a pivotal role in efficient SHG, which is achieved by perfect phase-matching including momentum conservation and energy conservation. The former can be fulfilled by a pair of modes with proper angular momentum relation $m_2 = 2m_1$, where m_1 (m_2) is the angular number of the pump (SH) cavity mode. However, the material and geometric dispersion presents a challenge on energy conservation, obstructing the double resonance $\omega_2 = 2\omega_1$ and consequently, efficient SHG. More accurately, the SH power can be derived from coupled mode equations (see Supplementary Information)

$$P_2 = \frac{4|g|^2 Q_2^2/(\omega_2 Q_{1e})}{4Q_2^2(2\omega_p/\omega_2 - 1)^2 + 1} \frac{16 Q_1^4 P_1^2/(\omega_1 Q_{2e})^2}{[4Q_1^2(\omega_p/\omega_1 - 1)^2 + 1]^2}, \tag{1}$$

where the subscripts 1, 2 represent the pumped mode and SH mode respectively. ω_i is the mode frequency and ω_p is the pump frequency. P_1 denotes the input pump power, g is the coupling coefficient between two modes, Q_i ($i = 1, 2$) stands for the loaded quality factor and Q_{ie} represents the external quality factor. The pump power depletion is ignored due to the weak second order nonlinear effect in silica. Eq. (1) shows that ultrahigh Q is indispensable in boosting the SH power, while it also presents a challenge in double resonance by magnifying the frequency mismatch induced by the material and geometric dispersion. In order to compensate the dispersion, SH modes with higher order radial number was proposed or used [3][Levy], which relies on delicate geometric design of the cavity. In the experiment, however, the desired phase-matching can be disturbed by the deviation of cavity from its designed geometry, making one of the mode off-resonance and impeding highly efficient SHG. Therefore, to tune the cavity dispersion precisely and dynamically, we propose and experimentally realize a versatile method, leveraging mode frequency shift induced by thermal behavior (namely thermal expansion, thermally induced refractive index change and the optical Kerr effect) [4, 5].

The mechanism of thermal and Kerr assisted phase matching process is illustrated in fig.2a. When the pump power is weak and the mode frequency shift is negligible (cold cavity), the pumped (ω_{10}) and SH modes (ω_{20}) usually cannot be on resonance with the pump light and its SH simultaneously. With a larger input

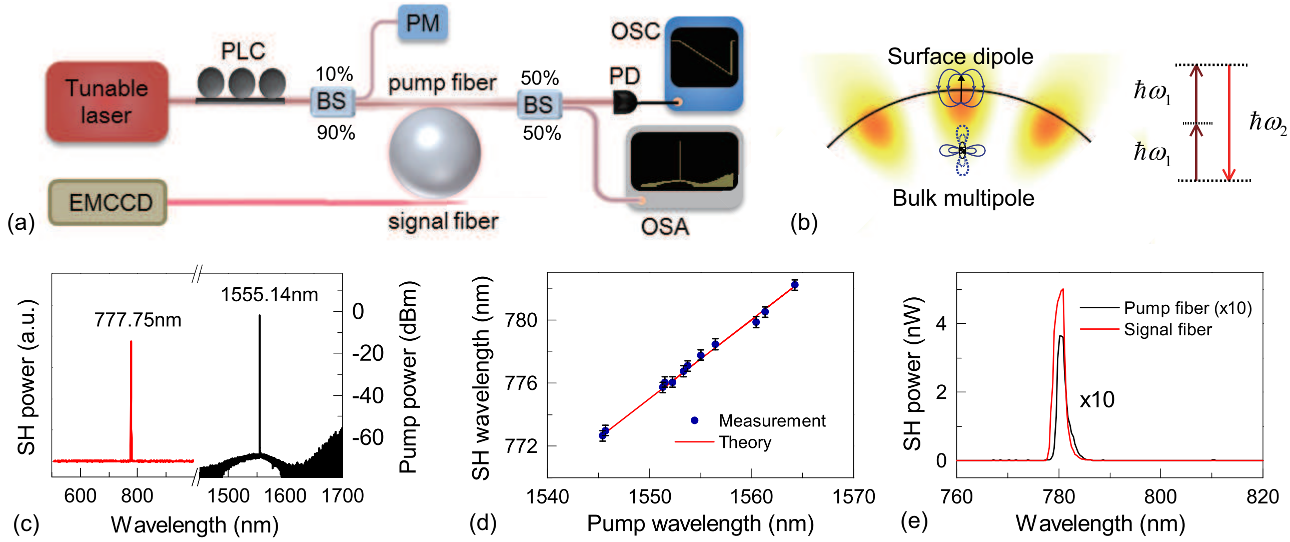

Figure 1: **Experimental set-up and observation of cavity-enhanced SH signals. a,** The pump light from a tunable laser around 1550 nm is coupled into a silica microsphere through a tapered fiber, and a second fiber is used to collect the SH signal. OSC: oscilloscope. OSA: optical spectrum analyzer. PLC: polarization controller. BS: beam splitter. EMCCD: electron-multiplying CCD. **b,** SH is generated from the surface dipole response and the bulk multipole response in a WG microsphere. **c,** Measured SH spectrum (red) and the corresponding pump spectrum (black). **d,** Measured SH wavelengths versus the corresponding pump wavelengths when different modes are pumped. **e,** Comparison of SH power collected by signal fiber and pump fiber (10 times magnified).

power, the pump mode experiences a red shift due to xxx: $\omega_1 = \omega_{10} - B_{11}|\alpha_1|^2$, where $|\alpha_1|^2$ is the intra-cavity power of the pumped mode and B_{11} is the coefficient of pump frequency shift. In this case, the wavelength of pump light should also increase to catch the pump mode, resulting in the non-Lorentzian, triangular transmission shape [carmon2004]. The SH mode also exhibits a red shift from cold cavity frequency, which can be described by $\omega_2 = \omega_{20} - B_{12}|\alpha_1|^2$ where B_{12} is the coefficient of SH frequency shift. The thermal and Kerr effects of the SH is ignored in the analysis. In the process of tuning pump frequency from the cold cavity mode to resonance (state 1-3 in fig.2a), the larger rate of red shift for the SH of pump light ($\omega_p/2$) helps it to catch the SH mode (ω_2) at a certain pump-cavity detuning where the phase-matching condition is fulfilled the SH power reaches a peak value (state 2). Because of the ultrahigh Q of the SH resonance, the SH power diminishes rapidly before and after reaching the on-resonance frequency for SH (state 1 and 3 in fig.2a and b). xxx phase matching can also be realized in other cases with different rate of SH mode frequency shift or initial detuning between $\omega_p/2$ and ω_2 (see SI).

Using the phase matching method, we measure the SH power by tuning the pump frequency in the range of the gray area (fig. 2b) with a fixed input power, as shown in fig. 2c.Furthermore, the dependence of SH power on pump power is also studied, as presented in fig.2d. Under each input power, we search for the maximum SH output power in the detuning range from the cold cavity mode to the on-resonance frequency for the pump. Among different values of input power, a critical power manifests itself, at which the SH of pump light achieves resonance condition exactly when the pump becomes completely resonant. In this case, the SH power is able to arrives at the peak value in fig. 2c, which represents the most efficient SHG with the pump power of 879 μW and the conversion efficiency of 0.049% W^{-1}. Below the critical power, the SH of pump light is off resonance within the full detuning range, resulting in the extremely weak SH power. Above the critical power, the increasing input power at a fixed frequency pushes the pump mode farther to the red side (the pump is not completely on resonance) and consequently increases the detuning between the pump light and the cavity. The resulting reduced enhancement of the pump light counteracts with the increasing input power, leading to the almost steady intracavity power. [SI] The on-resonance frequency of the SH mode also remains unchanged with increasing input power, so that the intracavity power and consequently the SH power are almost unchanged as well.

Microresonator SHG in other materials usually use different phase matching strategy to achieve broadband phase matching, e.g. quasi-phase-matching [cite more later]. The quality factor is also moderate so that the thermal effect and Kerr effect do not manifest themselves in the SHG process. With xxx phase matching, it is also possible to obtain the explicit $P_2 \propto P_1^2$ dependence by introducing a degree of freedom other than the pump intracavity power to manipulate the SH mode frequency. For example, a control light or a heater can be incorporated into the system to change the intra-cavity power and thus achieving the double on-resonance condition at various input pump power. The specific measurement plan is beyond the scope of this [letter?].

Apart from the unique power response, the SH power enhanced by the microresonator also exhibits a polarization dependence. In the experiment, transverse magnetic (TM) or transverse electric (TE) modes from 1545 nm to 1565 nm are pumped separately by adjusting the polarization of the pump light. The maximum SH power

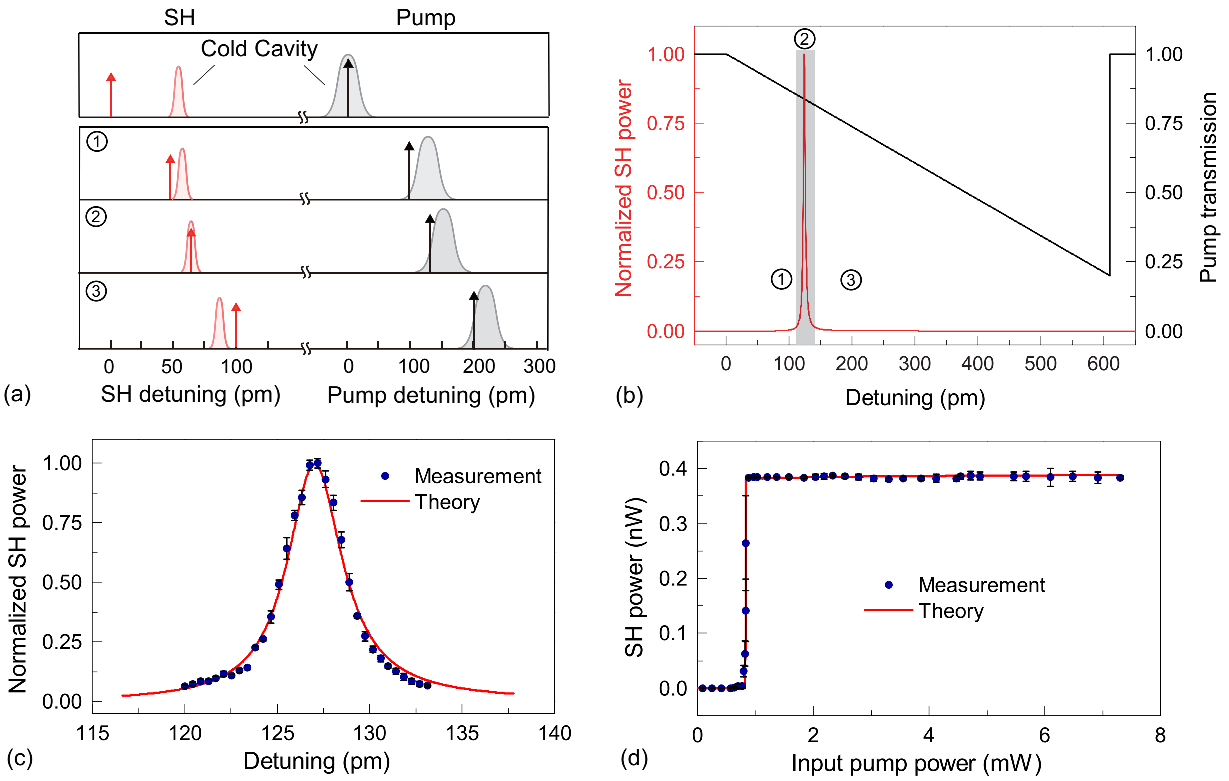

Figure 2: **Thermal effect and Kerr effect assisted phase-matching.** **a,** Schematic of the phase-matching process. Detuning here is the wavelength relative to the cold-cavity wavelength of the pumped mode (to half of this wavelength for SH detuning). The black (red) arrow represents the detuning of the pump light (its SH). The gray (red) Lorentzian line represents the pumped mode (SH mode). 1-3 show three states with increasing pump wavelength but the same input power. **b,** Normalized SH power and the pump transmission at different pump wavelength detuning. 1-3 correspond to the three states in panel **a**. The gray area is enlarged in panel **c** as the theoretical red line. **c,** SH power versus pump detuning with the input power of 4.46mW. **d,** The dependence of maximum SH power at all the pump detuning on the input power.

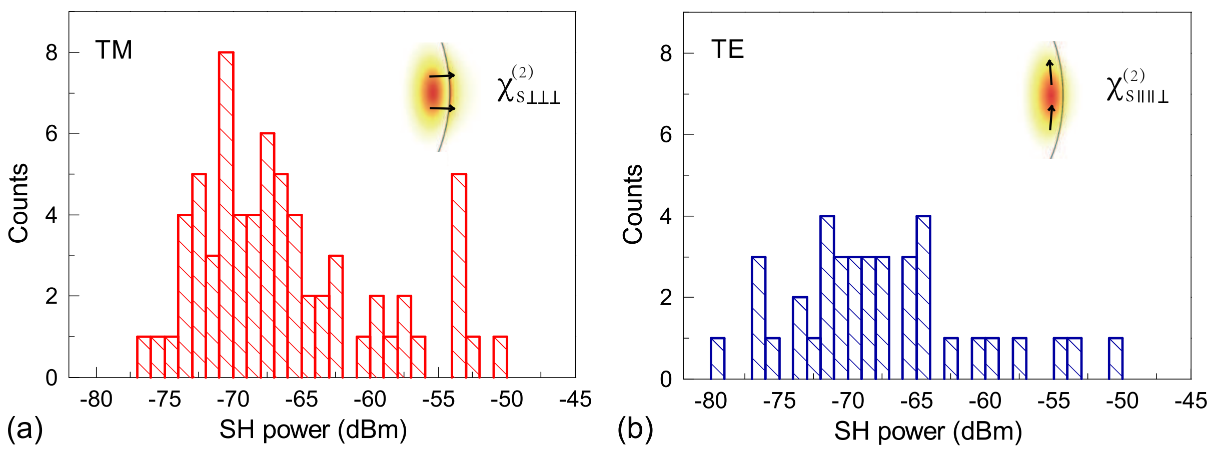

Figure 3: **SH power histogram with different pump polarization.** **a,** TM and **b,** TE modes are pumped to generate SH respectively. Insets: Field amplitude distribution and the direction of the electric field (black arrow).

of each SHG process is recorded for the two polarization respectively, as shown in the histogram in fig. 3. After traversing the wavelength range with each polarization, a total number of 69 (40) SHG incidence is recorded for TM (TE) polarization, and the average SH power is 0.843 nW (0.619 nW). The dependence on polarization originates from the nonlinear coupling strength g in eq.(1), which can be derived from the Helmholtz equation and the relation between electric field and nonlinear polarization. The second order nonlinear coupling arises from the breaking inversion symmetry at the surface and the bulk multipole response. The surface nonlinear coupling strength can be written as

$$g_{s0} = 2\frac{\omega_1^2}{\omega_2 n^2}\frac{\int_{\text{surface}} \mathbf{E}_{02}^* : \chi_{s0}^{(2)} : \mathbf{E}_{01}\mathbf{E}_{01}\mathrm{d}\mathbf{S}}{\int |\mathbf{E}_{02}|^2\mathrm{d}\mathbf{V}} \tag{2}$$

where n is the refractive index, $\chi_{s0}^{(2)}$ represents the surface nonlinear susceptibility, and $\mathbf{E}_{0i}(\mathbf{x})$ denotes the normalized electric field. The bulk multipole nonlinear polarization in silica can be expressed as $\mathbf{P}^{\text{bulk}} = \gamma\nabla(\mathbf{E}\cdot\mathbf{E}) + \delta(\mathbf{E}\cdot\nabla)\mathbf{E}$ [ref], where γ and δ are the nonlinear coefficients. The first term $\mathbf{P}_\gamma^{\text{bulk}}$ represents a longitudinal wave which can excite SH only at the surface. Therefore $\mathbf{P}_\gamma^{\text{bulk}}$ can contribute to an effective surface susceptibility $\chi_s^{(2)} = \chi_{s0}^{(2)} + \chi_{s,\gamma}^{(2)}$[6], corresponding to an effective coupling strength of g_s. The coupling strength induced by the second term $\mathbf{P}_\delta^{\text{bulk}}$ can be written as

$$g_b = 2\frac{\omega_1^2\delta}{\omega_2 n^2}\frac{\int \mathbf{E}_{02}^* \cdot (\mathbf{E}_{01}\cdot\nabla)\mathbf{E}_{01}\mathrm{d}\mathbf{V}}{\int |\mathbf{E}_{02}|^2\mathrm{d}\mathbf{V}} \tag{3}$$

Thus the total second order nonlinear coupling strength $g = g_s + g_b$.

The effective surface susceptibility tensor $\chi_s^{(2)}$ contains three non-zero components $\chi_{\perp\perp\perp}$, $\chi_{\parallel\parallel\perp}$ and $\chi_{\perp\parallel\parallel}$, where $\perp$ denotes the electric field direction perpendicular to the surface and $\parallel$ corresponds to the parallel direction. $\chi_{\perp\parallel\parallel}$ can be ignored in studying SHG due to the nondegeneracy of TM and TE pump modes. $\chi_{\perp\perp\perp}$ ($\chi_{\parallel\parallel\perp}$) plays a major role when TM (TE) mode is pumped, which only generates the TM polarized second harmonic in both cases. TM modes are preferable in surface induced SHG because $\chi_{\perp\perp\perp}$ is larger than $\chi_{\parallel\parallel\perp}$ [7]. Considering the bulk nonlinear response induced by $\mathbf{P}_\delta^{\text{bulk}}$, the coupling strength g_b relies on the specific field distribution in the cavity and the generated SH exhibits the same polarization as the pump mode. Note that for TE polarization, the field direction is along the polar direction, so that the polar symmetry of modes prohibits the excitation of SH modes with an even polar distribution from $\mathbf{P}_\delta^{\text{bulk}}$. While the TM pump modes, with electric field along the radial direction, can excite second harmonic without the above restriction. Because of a stronger confinement in the radial direction than the polar direction and thus a larger divergence for most of the modes, TM modes tend to link with a larger g_b than TE modes. Consequently, from both the surface and the bulk second order nonlinearity, TM pump modes can generate stronger SH signals statistically, which agrees with the measurement shown in fig. 3

The polarization dependence can be utilized to add to the surface specificity for SHG sensing, where the bulk nonlinear response of both $\mathbf{P}_\gamma^{\text{bulk}}$ and $\mathbf{P}_\delta^{\text{bulk}}$ should be eliminated. The former effect does not contribute to susceptibility $\chi_{\parallel\parallel\perp}$, corresponding to the TE polarized pump [heinz]. The latter can also be discerned from the surface nonlinear response with the TE polarized pump. In this case, an SH signal with a TM polarization can only originate from the surface nonlinearity ($\chi_{\parallel\parallel\perp}$) because $\mathbf{P}_\delta^{\text{bulk}}$ requires the same polarization between the pump mode and the SH mode. Furthermore, when a fundamental [] TE mode ($l_1 = m_1$) is pumped, only the fundamental SH modes ($l_2 = m_2$) are allowed by the selection rule [], which cannot be excited from $\mathbf{P}_\delta^{\text{bulk}}$ due to even polar field distribution of the SH mode. In the experiment, we employ a fundamental TE pump mode at xx nm and obtain a surface-only second harmonic deterministically without measuring the SH polarization.

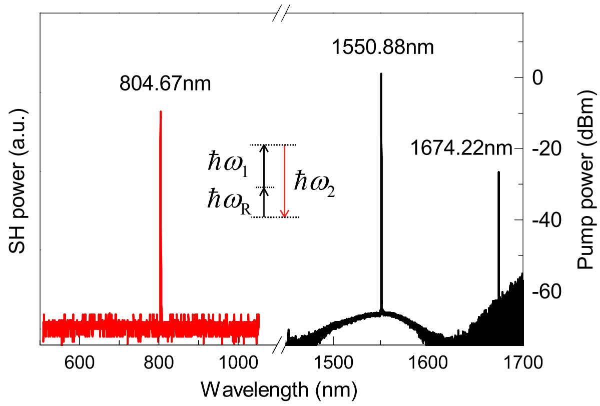

Figure 4: **Measured spectra of second-order sum frequency generation (SFG).** The pump light (ω_1) and Raman light (ω_2) are summed to generate the SF signal (ω_3).

Additionally, sum frequency generation (SFG) can also arise when a Raman signal is stimulated by the pump light. Shown in fig.4 is an SF signal (804.67 nm) and the corresponding pump (1550.88 nm) and its Raman signal (1674.22 nm) with an input power of 7.33 mW, which is above the Raman threshold for this mode. The deviation of the SF wavelength from the expected value (804.63 nm) is much smaller than the resolution of EMCCD.

[Conclusion]

References

[1] J Cheung Knight, G Cheung, F Jacques, and TA Birks. Phase-matched excitation of whispering-gallery-mode resonances by a fiber taper. *Optics letters*, 22(15):1129–1131, 1997.

[2] Ming Cai, Oskar Painter, and Kerry J Vahala. Observation of critical coupling in a fiber taper to a silica-microsphere whispering-gallery mode system. *Physical review letters*, 85(1):74, 2000.

[3] Gregory Kozyreff, JL Dominguez Juarez, and Jordi Martorell. Whispering-gallery-mode phase matching for surface second-order nonlinear optical processes in spherical microresonators. *Physical Review A*, 77(4):043817, 2008.

[4] Pascal DelHaye, T Herr, E Gavartin, ML Gorodetsky, Ronald Holzwarth, and Tobias J Kippenberg. Octave spanning tunable frequency comb from a microresonator. *Physical Review Letters*, 107(6):063901, 2011.

[5] T Herr, V Brasch, JD Jost, CY Wang, NM Kondratiev, ML Gorodetsky, and TJ Kippenberg. Tem-

poral solitons in optical microresonators. *Nature Photonics*, 8(2):145–152, 2014.

[6] Tony F Heinz. Second-order nonlinear optical effects at surfaces and interfaces. *Nonlinear surface electromagnetic phenomena*, 29, 1991.

[7] Francisco J Rodriguez, Fu Xiang Wang, and Martti Kauranen. Calibration of the second-order nonlinear optical susceptibility of surface and bulk of glass. *Optics express*, 16(12):8704–8710, 2008.